Derivative-Hilbert-Backprojection-based image reconstruction from truncated projections in helical cone-beam CT postprint

Authors: ZHANG Feng, YAN Bin, LI Lei, XI Xiao-Qi, JIANG Hua, WEI Xing, ZHANG Xiang, CUI Jin-Xian

Date: 2023-06-18T00:00:00+00:00

Abstract

In helical cone-beam computed tomography (CT), Feldkamp-Davis-Kress (FDK) based image reconstruction algorithms are by far the most popular. However, artifacts are commonly met in the presence of lateral projection truncation. The reason is that the ramp filter is global. To restrain the truncation artifacts, an approximate reconstruction formula is proposed based on the Derivative-Hilbert-Backprojection (DHB) framework. In the method, the first order derivative filter is followed by the Hilbert transform. Since the filtered projection values are almost zero by the first order derivative filter, the following Hilbert transform has little influence on the projection values, even though the projections are laterally truncated. The proposed method has two main advantages. First, it has comparable computational efficiency and image quality as well as the conventional helical FDK algorithm for non-truncated projections. The second advantage is that images can be reconstructed with acceptable quality and much lower computational cost in comparison to the Laplace operator based algorithm in cases with truncated projections. To point out the advantages of our method, simulations on the computer and real data experiments on our laboratory industrial cone-beam CT are conducted. The simulated and experimental results demonstrate that the method is feasible for image reconstruction in the case of projection truncation.

Full Text

Preamble

Derivative-Hilbert-Backprojection-based image reconstruction from truncated projections in helical cone-beam CT

Feng Zhang, Bin Yan†, Lei Li, Xiao-Qi Xi, Hua Jiang, Xing Wei, Xiang Zhang, and Jin-Xian Cui

National Digital Switching System Engineering & Technology Research Center, Zhengzhou 450002, China

(Received April 11, 2014; accepted in revised form May 15, 2014; published online April 20, 2015)

Abstract: In helical cone-beam computed tomography (CT), Feldkamp-Davis-Kress (FDK) based image reconstruction algorithms are by far the most popular. However, artifacts are commonly encountered in the presence of lateral projection truncation because the ramp filter is global. To restrain these truncation artifacts, we propose an approximate reconstruction formula based on the Derivative-Hilbert-Backprojection (DHB) framework. In our method, a first-order derivative filter is followed by the Hilbert transform. Since the filtered projection values are almost zero after the first-order derivative filter, the subsequent Hilbert transform has little influence on the projection values even when the projections are laterally truncated. The proposed method offers two main advantages. First, it achieves computational efficiency and image quality comparable to the conventional helical FDK algorithm for non-truncated projections. Second, it can reconstruct images with acceptable quality at much lower computational cost compared to Laplace operator based algorithms when dealing with truncated projections. To demonstrate these advantages, we conducted both computer simulations and real data experiments on our laboratory industrial cone-beam CT system. The simulated and experimental results confirm that our method is feasible for image reconstruction in cases of projection truncation.

Keywords: Helical cone-beam CT, Image reconstruction, Truncation artifacts, Derivative-Hilbert-Backprojection

DOI: 10.13538/j.1001-8042/nst.26.020401

Introduction

In cone-beam computed tomography, helical scans offer the advantages of higher scanning speed and more uniform axial sampling compared to circular scans [**?**]. The image reconstruction problem for helical scans has been well addressed through both approximate and exact algorithms [**?**]. Among these methods, the approach by Wang et al. [**?**] (hereafter called the helical FDK method) is computationally efficient and widely used in practice. However, this method is only suitable when the object under investigation fits within the field of view (FOV) defined by the detector size, scan magnification, and rotation axis location. When the object exceeds the FOV, the sampled projections become truncated and the method faces significant challenges. When projections are truncated on both sides—the interior problem—image reconstruction has been proven to have no unique or stable solutions [**?**]. If the helical FDK method is applied to truncated projections, the resulting image quality is severely degraded

by truncation artifacts [**?**].

Recent developments in local reconstruction algorithms have provided new solutions to the interior problem [**?**]. Among these solutions, the approximate truncation reconstruction computed tomography (ATRACT)-type algorithms developed by Dennerlein et al.' s group are highly practical [**?**]. The main idea is to replace the ramp filter in FDK-type algorithms with a cascade of local and global filters [**?**, **?**]. This approach aims to retain the advantages of high computational efficiency and low resource demand characteristic of FDK-type methods. Building on Dennerlein et al.' s work, Zou et al. [**?**] recently proposed a general Laplace operator based reconstruction algorithm (LORA) for helical scans (called the Laplace operator based method in this paper), which uses the Laplace operator and 2D Radon-based filters as the local and global filters, respectively. Although this method can provide better reconstruction than the helical FDK algorithm for truncated spiral cone-beam CT, the Radon-based filter is computationally expensive. Numerous improvements have been made to enhance computational efficiency since Dennerlein et al.'s initial work [**?**, **?**, **?**, **?**]. Among these, Wang et al. [**?**] proposed filtering projections using first-order derivative and Hilbert filters, which can be described as the Derivative-Hilbert-Backprojection (DHB) framework. This method is outstanding in terms of both computational cost and image quality.

In this paper, we propose a novel approximate reconstruction formula based on Wang et al.' s results for truncated projections in helical cone-beam CT. The remainder of the paper is organized as follows. Section II describes the geometry of helical scanning. Section III introduces our method in detail. Section IV presents numerical simulation and experimental results. Section V provides concluding remarks.

II. Notation and Basic Definitions

The helical scan geometry is illustrated in Fig. 1 [FIGURE:1]. Without loss of generality, we assume the X-ray source and flat panel detector rotate around the imaging object during data acquisition. The source position, parameterized by the azimuth angle $\lambda \in \mathbb{R}$, is denoted by $\vec{r}_0(\lambda)$. Three coordinate systems are used in this geometry. The first is the 3-dimensional Cartesian coordinate system $Oxyz$, which is fixed in the helical scan. The second is the rotational coordinate system spanned by $\vec{e}_u(\lambda) = (-\sin\lambda, \cos\lambda, 0)$, $\vec{e}_\nu(\lambda) = (0, 0, 1)$, and $\vec{e}_w(\lambda) = (\cos\lambda, \sin\lambda, 0)$. The third is the 2-dimensional Cartesian coordinate system on the flat detector with u- and ν-axes.

For a helical trajectory with constant pitch h and constant radius R, the source position is $\vec{r}_0(\lambda) = (R\cos\lambda, R\sin\lambda, h\lambda/(2\pi))$. The pitch is defined as the axial distance between two points on the helix separated by exactly one turn. The flat panel detector is arranged parallel to vectors $\vec{e}_u(\lambda)$ and $\vec{e}_\nu(\lambda)$, and orthogonal to vector $\vec{e}_w(\lambda)$. The distance from the source to the flat panel detector is D, and R represents the distance between the source and the rotation axis. The

FOV of helical cone-beam CT is a bounding cylinder C.

We assume the spatial distribution of the X-ray absorption coefficient of the imaging object is a compact function denoted by $f(\vec{r})$, bounded by Ω. The projection of object $f(\vec{r})$ onto the flat panel detector is

$$g(\lambda, u, \nu) = \int f(\vec{r}_0(\lambda) + \vec{\theta}t)\, dt$$

The X-ray direction given by parameters λ, u, and ν is defined by

$$\vec{\theta} = \frac{u\vec{e}_u(\lambda) + \nu\vec{e}_\nu(\lambda) - D\vec{e}_w(\lambda)}{\sqrt{u^2 + \nu^2 + D^2}}$$

where the detector coordinates (u, ν) of the intersection where the X-ray passing through $\vec{r} = (x, y, z)$ hits the detector can be computed as

$$u = \frac{\vec{r} \cdot \vec{e}_u(\lambda)}{R - \vec{r} \cdot \vec{e}_w(\lambda)} D \quad \text{and} \quad \nu = \frac{\vec{r} \cdot \vec{e}_\nu(\lambda)}{R - \vec{r} \cdot \vec{e}_w(\lambda)} D$$

If the object $f(\vec{r})$ cannot be laterally surrounded by the FOV of a helical scan (i.e., Ω cannot be contained by C), the captured projection is laterally truncated.

III. Theory

To obtain better image quality from transversely truncated projections in a helical trajectory, we propose a novel reconstruction algorithm based on Wang et al.' s work. The new reconstruction formula can be written as

$$f(\vec{r}) = \int_\theta^{\theta+\pi} \frac{1}{[R - \vec{r} \cdot \vec{e}_w(\lambda)]^2} \left[\int_{-\infty}^{\infty} h_H(u - u') \left[\frac{D^2 + u^2 + \nu^2}{D^2} g(\lambda, u, \nu) \right] du' \right] d\lambda$$

where $\theta = 2\pi z/h$. Formula (4) can be implemented in four steps:

Step 1. Weight the projection data:

$$g_1(\lambda, u, \nu) = \frac{D^2 + u^2 + \nu^2}{D^2} g(\lambda, u, \nu)$$

where $g(\lambda, u, \nu)$ is the projection at view angle λ and (u, ν) is a detector pixel coordinate.

Step 2. Compute the first-order derivative of the weighted projection with respect to u:

$$g_2(\lambda, u, \nu) = \frac{\partial}{\partial u} g_1(\lambda, u, \nu)$$

Step 3. Apply Hilbert filtering to $g_2(\lambda, u, \nu)$ row by row:

$$g_3(\lambda, u, \nu) = g_2(\lambda, u, \nu) * h_H(u)$$

where $h_H = 1/(\pi u)$ is the Hilbert transform kernel and $*$ denotes convolution.

Step 4. Back-project the filtered projections onto the 3D volume:

$$f(\vec{r}) = \int_{\theta}^{\theta+\pi} \frac{1}{[R - \vec{r} \cdot \vec{e}_w(\lambda)]^2} g_3(\lambda, u, \nu) d\lambda$$

Mathematically, formula (4) is equivalent to formula (10) in reference [**?**]. In the helical FDK algorithm, the filtration kernel $|\omega|$ is ramp-like in the frequency domain. In our method, the ramp filter is replaced by a cascade of first-order derivative and Hilbert operators. Hence, the proposed reconstruction method has the same characteristics as the helical FDK algorithm for global reconstruction. To obtain correct filtered results, the acquired projection must be complete because $|\omega|$ is global. When projections are transversely truncated, the filtered values differ from those obtained from non-truncated projections, resulting in truncation artifacts in the reconstructed image. However, the filtered projection values $g_2(\lambda, u, \nu)$ produced by the first-order derivative operator are close to zero in most regions. Even though the subsequent Hilbert filter remains global, the final filtered errors are significantly reduced compared to the helical FDK algorithm.

Unlike our method, Zou et al.' s approach utilizes the Laplace operator and 2D Radon-based filters [**?**]. After obtaining the weighted projection $g_{\text{Zou}}(\lambda, u, \nu)$, Zou et al. perform Laplace operator based filtering:

$$g_{\text{Laplace}}(\lambda, u, \nu) = \left(\frac{\partial^2}{\partial u^2} + \frac{\partial^2}{\partial \nu^2} \right) g_{\text{Zou}}(\lambda, u, \nu)$$

and 2D Radon-based filtering:

$$F(\lambda, u, \nu) = -\int_0^{\pi} |\cos \mu| g_{\text{Zou}}(\lambda, u, \nu) d\mu$$

where

$$g_{\text{Radon}}(\lambda, u^*, \nu^*) = \int g_{\text{Zou}}(\lambda, u, \nu) \delta(u \cos \mu + \nu \sin \mu - s) du d\mu$$

is the Radon transform, with $s = u^* \cos\mu + \nu^* \sin\mu$. In implementing the 2D Radon-based filter, the discretizations of s and λ (denoted by Δs and $\Delta\lambda$, respectively) are critical to filtered projection quality. Obviously, smaller values of Δs and $\Delta\lambda$ yield better filtered projection quality but demand more computation time. In our following discussions, $\Delta s = 0.5$ pixel and $\Delta\lambda = 0.5^\circ$.

To compare filtered results from the three reconstruction methods, we generated and filtered both non-truncated 2D Shepp-Logan phantoms (512×512 pixels) and truncated versions (256×512 pixels). Figure 2 [FIGURE:2] shows the filtered results for the non-truncated phantom. The filtered image using Zou et al.' s method exhibits a jagged shape, while our method' s result essentially coincides with that obtained using the ramp filter in the helical FDK algorithm.

Figure 3

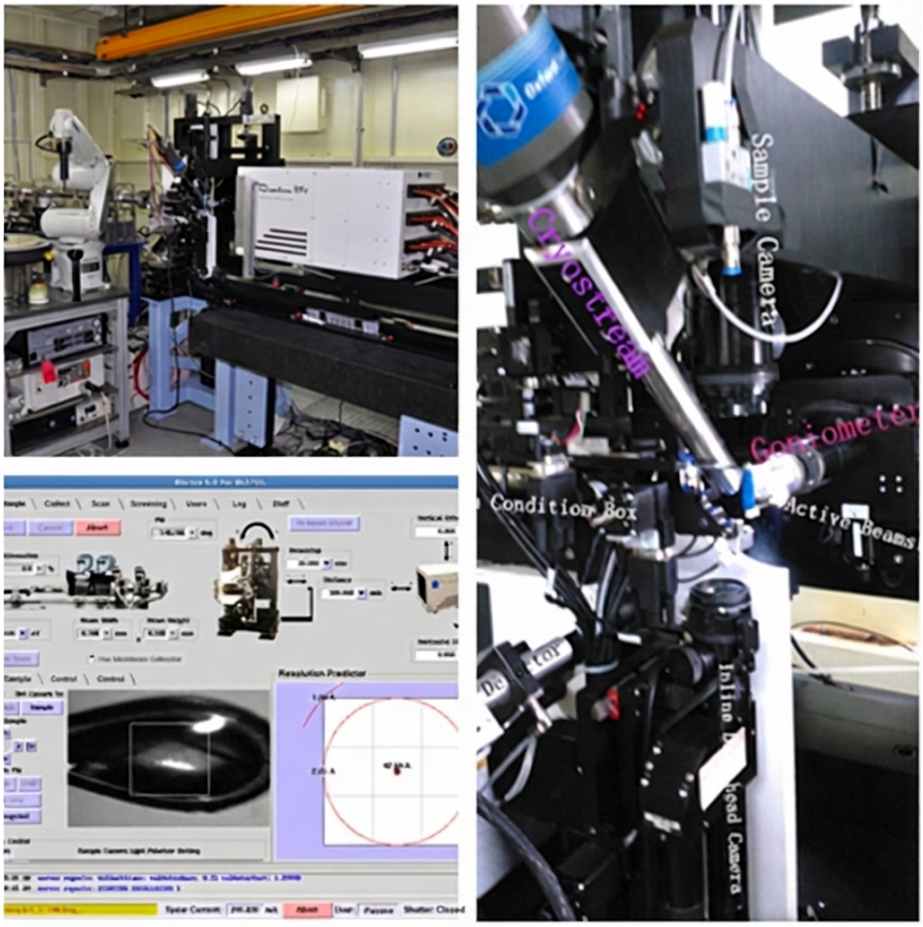

Figure 1: Figure 3

shows filtered results for the truncated phantom. Because the phantom image is incomplete, the helical FDK algorithm' s filtered image deviates from the true values, particularly at the truncated boundaries. As in the first simulation, Zou et al.' s method produces a jagged result, while our method agrees well with the true values.

Notably, filtering a 512×512 image with Zou et al.' s method consumes 25.609 s, and 15.703 s for a 256×512 image. In contrast, our method consumes only 0.204 s and 0.109 s respectively, while the helical FDK algorithm consumes 0.094 s and 0.046 s. These results demonstrate that our method offers significant time savings over Zou et al.' s method and higher quality than the helical FDK algorithm for truncated projections.

The DHB-based reconstruction method was proposed long ago, but at that time the first-order derivative was considered sensitive to noise and detrimental to reconstruction quality. Consequently, researchers preferred filtered back-projection (FBP) over DHB. To implement the DHB-based method in practice, we perform projection preprocessing such as denoising to suppress projection noise before reconstruction.

IV. Experiments and Discussions

A. Simulated Data

To verify the efficiency of our proposed method, we conducted numerical simulations and real data experiments, applying the helical FDK algorithm, Zou et al.' s method, and our method to the acquired projections. All algorithms were implemented on an HP workstation with 32 GB memory and an Intel E5-2620 CPU, programmed in C++ using Microsoft Visual Studio.

We demonstrated our method' s efficiency using simulated projection data from the 3D Shepp-Logan phantom [**?**]. The phantom size was 25.6 mm $\times$ 25.6 mm $\times$ 25.6 mm. We examined image reconstruction from both non-truncated (Simulation 1) and truncated projections (Simulation 2).

In Simulation 1, we generated non-truncated projections along a helical trajectory with parameters shown in the second column of TABLE 1 . The reconstruction matrix was $512 \times 512 \times 512$ with voxel edge length 0.05 mm along each axis. Figure 4 [FIGURE:4] shows the reconstruction images from the simulated non-truncated projections. Figure 5 [FIGURE:5] illustrates profiles through the middle row of the first slice in Fig. 4. All three methods produced high-quality reconstructions for non-truncated projections. However, the Laplace operator based method yields a jagged profile, while our method provides slightly superior reconstruction quality compared to Zou et al.' s method. Quantitative analysis using root mean square errors (RMSEs) relative to the phantom yielded values of 1.128×10^{-4}, 1.149×10^{-4}, and 1.147×10^{-4} for the three methods, respectively. TABLE 2 shows the computation time for reconstructing a 512×512 pixel slice. Zou et al.' s method is the most time-consuming, while our method requires

slightly more time than the helical FDK algorithm due to the computationally demanding 2D Radon-based filtering, as noted in Section III.

In Simulation 2, we generated truncated projections along the same helical trajectory with parameters shown in the third column of TABLE 1. The reconstruction matrix was $256 \times 256 \times 512$ with voxel edge length 0.05 mm. During filtering, the mean value of the truncated projection data was removed by both Zou et al.' s method and our method, which can cause offset or bias-like artifacts. For fair comparison, we applied scaling and offset corrections to the reconstruction images from both methods, following the techniques described in reference [**?**]. Figure 6 [FIGURE:6] shows the reconstruction images from the simulated truncated projections. The helical FDK algorithm' s result is severely contaminated by truncation artifacts. While Zou et al.' s method provides slightly better edge quality because Laplace operator filtered values are closer to zero than those from the first-order derivative filter, our method achieves superior overall performance. Quantitative evaluation using signal-to-noise ratio (SNR) in the region of interest (ROI, shown by the white circle in Fig. 6) yielded values of 10.38 dB, 19.54 dB, and 21.18 dB for the helical FDK algorithm, Zou et al.' s method, and our method, respectively. Computation times for reconstructing a 256×256 pixel slice are shown in TABLE 2, confirming similar conclusions to Simulation 1.

B. Real Data

Real data experiments were conducted on our laboratory industrial cone-beam CT system, consisting of a micro-focus X-ray source (FXT-225.48, Yxlon, Germany), a high-precision manipulator, and a flat panel detector with 2304×3200 pixels (4030E, Varian, USA). We scanned a car spark plug along a helical trajectory with source-to-object distance 125 mm, source-to-detector distance 1000 mm, helical pitch 36 mm, and 360 projections per turn at 0.127 mm/pixel resolution. With 3 turns, we collected 1080 projections. To avoid geometric artifacts, we first corrected the sampled projections using a practical geometric calibration method [**?**].

Although the collected projections were non-truncated (since the true values from the spark plug were unknown), we used the helical FDK reconstruction from these projections as the ground truth. The reconstructed 3D volume contained $1536 \times 1536 \times 5120$ voxels at 0.018 mm $\times$ 0.018 mm $\times$ 0.018 mm resolution. Figure 7 [FIGURE:7] shows a photo of the spark plug and the reconstruction images.

To evaluate performance on truncated projections, we virtually cropped the central 512 columns from all projections. We then applied the helical FDK algorithm, Zou et al.' s method, and our method to these cropped projections. The reconstruction matrix was $512 \times 512 \times 5120$ with voxel size 0.018 mm $\times$ 0.018 mm $\times$ 0.018 mm. Figures 8 and 9 [FIGURE:8, FIGURE:9] show slices at $y = 256$ and $z = 2400$, respectively. The helical FDK algorithm' s result

is severely affected by truncation artifacts, while Zou et al.' s method and our method significantly reduce these artifacts and provide comparable image quality. SNR values in the ROI (shown by the white circle in Fig. 9) were 9.81 dB, 14.06 dB, and 23.06 dB for the three methods, respectively. As in the simulations, our method remained faster than Zou et al.' s method; computational time comparisons are omitted for brevity.

V. Conclusion

For global tomography, the helical FDK algorithm remains the most popular method for helical scan reconstruction. However, image quality is always degraded by truncation artifacts when projections are truncated. In this paper, we proposed a novel approximate reconstruction formula based on the DHB framework for helical interior cone-beam CT. Our method replaces the ramp filtering operation in the helical FDK algorithm with a cascade of first-order derivative filtering and Hilbert filtering. Because the intermediate filtered projection values from the first-order derivative filter are close to zero, the final filtered results are not significantly altered by the subsequent Hilbert filter. Theoretically, our method is identical to the helical FDK algorithm for non-truncated cases and thus shares the same advantages, such as low resource demand.

Comparisons with Zou et al.' s Laplace operator based method demonstrated that our method offers lower computational cost and comparable image quality, giving it significant practical value. Although the first-order derivative operation may make our method sensitive to noise, this potential weakness can be overcome in practice by introducing projection denoising techniques such as non-local means.

References

[1] Zhang F, Yan B, Li L, et al. Practical geometric calibration for helical cone-beam industrial computed tomography. J X-ray Sci Technol, 2014, 22: 19–35. DOI: 10.3233/XST-130406

[2] Wang G, Lin T H, Cheng P C, et al. A general cone-beam reconstruction algorithm. IEEE T Med Imaging, 1993, 12: 486–496. DOI: 10.1109/42.241876

[3] Katsevich A. A general scheme for constructing inversion algorithms for cone beam CT. Int J Math Math Sci, 2003, 21: 1305–1321. DOI: 10.1155/S0161171203209315

[4] Zou Y, Pan X and Sidky E Y. Theory and algorithms for image reconstruction on chords and within regions of interest. J Opt Soc Am A, 2005, 22: 2372–2384. DOI: 10.1364/JOSAA.22.002372

[5] Natterer F. The Mathematics of Computerized Tomography. American Society for Industrial & Applied Mathematics Press, 2001, 121–125. DOI: 10.1137/1.9780898719284

[6] Sharma K S, Holzner C, Vasilescu D M, et al. Scout-view assisted interior micro-CT. Phys Med Biol, 2013, 58: 4297–4314. DOI: 10.1088/0031-9155/58/12/4297

[7] Yu H Y and Wang G. Compressed sensing based interior tomography. Phys Med Biol, 2009, 54: 2791–2805. DOI: 10.1155/2009/125871

[8] Yang J, Yu H, Jiang M, et al. High order total variation minimization for interior tomography. Inverse Probl, 2010, 26: 035013. DOI: 10.1088/0266-5611/26/3/035013

[9] Jin X, Katsevich A, Yu H, et al. Interior tomography with continuous singular value decomposition. IEEE T Med Imaging, 2012, 31: 2108–2119. DOI: 10.1109/TMI.2012.2213304

[10] Dennerlein F. Cone-beam ROI reconstruction using the Laplace operator. 11th international meeting on Fully Three-dimensional image reconstruction in Radiology and Nuclear Medicine, 2011, 80–83.

[11] Xia Y, Maier A, Dennerlein F, et al. Efficient 2D filtering for cone-beam VOI reconstruction, Nuclear Science Symposium and Medical Imaging Conference (NSS/MIC), Anaheim, CA, October 27, 2012, 2415–2420. DOI: 10.1109/NSS-MIC.2012.6551549

[12] Dennerlein F and Maier A. Region-of-interest reconstruction on medical C-arms with the ATRACT algorithm, SPIE Medical Imaging 2012: Physics of Medical Imaging, San Diego, CA, February 2012, 83131B. DOI: 10.1117/12.913274

[13] Xia Y, Maier A, Hofmann H G, et al. Reconstruction from truncated projections in cone-beam CT using an efficient 1D filtering, SPIE Medical Imaging 2013: Physics of Medical Imaging, Lake Buena Vista, FL, February 2013, 86681C. DOI: 10.1117/12.2007484

[14] Dennerlein F and Maier A. Approximate truncation robust computed tomography–ATRACT. Phys Med Biol, 2013, 58: 6133–6148. DOI: 10.1088/0031-9155/58/17/6133

[15] Xia Y, Hofmann H, Dennerlein F, et al. Towards clinical application of a Laplace Operator-based region of interest reconstruction algorithm in C-Arm CT. IEEE T Med Imaging, 2014, 33: 593–606. DOI: 10.1109/TMI.2013.2291622

[16] Feldkamp L A, Davis L C and Kress J W. Practical cone-beam algorithm. J Opt Soc Am A, 1984, 1: 612–619. DOI: 10.1364/JOSAA.1.000612

[17] Grass M, Köhler T and Proksa R. 3D cone-beam CT reconstruction for circular trajectories. Phys Med Biol, 2000, 45: 329–347. DOI: 10.1088/0031-9155/45/2/306

[18] Zou X B, Yu H and Zeng L. Laplace operator based reconstruction algorithm for truncated spiral cone beam computed tomography. J X-ray Sci Technol, 2013, 21: 515–526. DOI: 10.3233/XST-130398

[19] Wang X C, Yan B, Li L, et al. Cone-beam local reconstruction based on a Radon inversion transformation. Chinese Phys B, 2012, 21: 8702. DOI: 10.1088/1674-1056/21/11/118702

[20] Toft P A. The Radon transform, theory and implementation. Ph.D. Thesis, Technical University of Denmark, 1996.

Figures

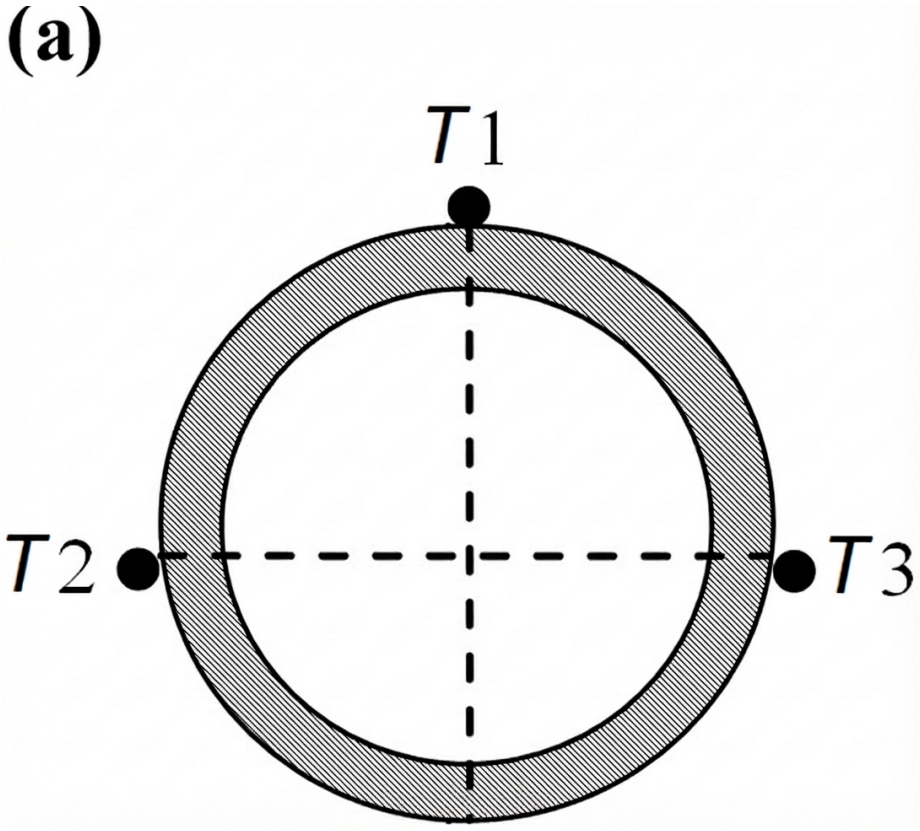

Figure 2: Figure 11

Figure 3: Figure 17